

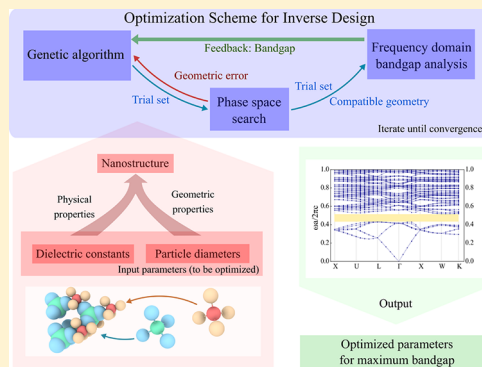
Investigation of Geometric Landscape and Structure–Property Relations for Colloidal Superstructures Using Genetic Algorithm

Nishan Parvez,[†] Dhananjai M. Rao,[‡] and Mehdi B. Zanjani^{*,†}

[†]Department of Mechanical and Manufacturing Engineering, Miami University, Oxford, Ohio 45056, United States

[‡]Department of Computer Science and Software Engineering, Miami University, Oxford, Ohio 45056, United States

ABSTRACT: Over the past two decades, colloidal particles with a variety of shapes, sizes, and compositions have been synthesized and characterized successfully. One of the most important applications for colloidal building blocks is to engineer functional structures as mechanical, electrical, and optical metamaterials. However, complex interaction dynamics between the building blocks as well as sophisticated structure–property relationships make it challenging to design structures with predictable target properties. In this paper, we implement an inverse material design framework using Genetic Algorithm (GA)-based techniques to streamline the design of colloidal structures based on target properties. We investigate spherical particles as well as colloidal molecules of different sizes and shapes and evaluate a Geometric Landscape Accessibility parameter that identifies the size of feasible domains within the geometric phase space of each structure. Considering target photonic properties, our GA-assisted framework is further utilized to identify sets of building blocks and structures that lead to various target values for the size of the photonic band gaps. The proposed framework in this study will provide new insight for predictive computational material design approaches and help establish more efficient ways of understanding structure–property relations in sub-micrometer-scale materials.



INTRODUCTION

Colloidal structures provide a versatile platform for engineering metamaterials with desired functionalities and tunable properties.^{1–6} Micro- and nanoscale colloidal building blocks of different sizes and shapes have been utilized to build a wide variety of colloidal structures.^{7–41} Predicting structural symmetries that can arise from different types of building blocks is an important topic that has attracted significant interest among material scientists.^{42–44} On the other hand, predicting and understanding different properties of colloidal structures is equally important for designing functional metamaterials for applications such as optical,^{28,45–48} thermal,^{49–51} and electronic devices.^{52,53} For this purpose, computational methods^{2,24,30,31} and machine learning techniques^{54–56} provide a useful platform to investigate and study colloidal structures and their properties.

One of the main challenges with the study of sub-micrometer colloidal systems is to design structures that will lead to specific desired properties. Traditional material design methods have mainly focused on studying and measuring the properties of existing materials and structures, which is a time-consuming task and is experimentally very expensive. A much more efficient method is to use an inverse material design platform that involves target properties driving the material design process. In this approach, desired material properties such as specific mechanical or optical characteristics are provided as input, and the output of the design process is to identify a set of building blocks that produce a material

structure with the specified target properties. However, considering the large library of available colloidal particles and structures, finding an optimized set of particles that will provide a structure with target properties is nontrivial. Specifically, two major obstacles come to mind. First, the building blocks possess a variety of geometric features and shapes. Even for a known structure symmetry, there are only a limited number of combinations of building block sizes and shapes that would result in the formation of the intended structure. This essentially means there are complex geometric constraints, unique to each structure, that limit the choice of the building blocks.^{2,30–32,57} Second, the connection between the properties of a colloidal construct and its structural features is in general very complicated and hard to predict.^{58,59} Therefore, sophisticated computational or experimental frameworks are needed to successfully establish an inverse material design approach.

In this paper, we develop a Genetic Algorithm-assisted framework to implement a property-driven material design approach for a wide range of colloidal building block types and structures. We first study the geometric landscape and analyze the geometric phase space for structures formed by colloidal particles of different sizes and shapes. We also demonstrate an effective way to navigate the complicated geometric landscape

Received: June 4, 2019

Revised: August 2, 2019

Published: August 2, 2019

when complex building blocks, such as multi-component colloidal molecules, are used. This leads to the identification of geometrically feasible domains within the geometric phase space for these structures, which we then quantitatively characterize by defining and calculating a Geometric Landscape Accessibility (GLA) parameter. Next, we explore structure–property relations for the structures studied in the previous step through the use of Genetic Algorithm (GA). Without loss of generality, we focus on the photonic properties and photonic spectrum of these materials. The GA finds the optimized values for different features of the building blocks, such as particle sizes and dielectric constants, for various structures, in order to achieve the target photonic properties. The results of this work provide a footprint for inverse material design approaches as well as a better understanding of the complex geometric landscapes and the intricate structure–property relations present in the design process of novel colloidal structures.

RESULTS AND DISCUSSION

Figure 1 shows a schematic of the implementation of our material design approach. In *traditional material design*, material properties are examined for previously established material structures with well-known building blocks. This approach limits material design since the existing materials, as well as newly discovered structures, may not possess desired properties even after considerable modifications. However, within the *inverse material design* approach, as shown in Figure 1a, desired properties are the major target of the design process, which would decide the choice of the building blocks and the suitable overall structure. Here we focus on the development of an integrated Genetic Algorithm-based inverse material design scheme, which couples predictive analysis of material properties with the self-assembly behavior of micro- or nanoscale colloidal particles. Figure 1b demonstrates various elements of this approach. Within this framework, optimization schemes are utilized to determine combinations of building blocks that self-assemble into structures with target properties. Figure 1c shows examples of different classes of sub-micrometer-scale building blocks that can be utilized to design materials with specific functionalities. These building blocks include single particles with spherical or nonspherical shapes,^{5,60,61} patchy particles,²⁶ and clusters of two or more particles,^{23,27} which provide a wide variety of structure symmetries for discovery of materials with specific properties through the inverse design approach.

Broadly speaking, the parameters associated with each structure can be classified into two categories: geometric and physical. Under the geometric parameter category, the shape and sizes of the elements of each building blocks are considered. Physical parameters include properties of the elementary particles of the building blocks that contribute to the problem-specific target properties of the overall structures. In general, the available parameter space will be very high dimensional, and establishing structure–property relations is a challenging task. For example, the geometric parameters of a system with two types of tetrahedral clusters, as shown in Figure 1c, includes four different particle sizes that can be changed independently. Only a limited number of combinations of these particle sizes will result in the formation of the desired structures. Identifying acceptable combinations of these parameters requires a full sweep of the parameter space,

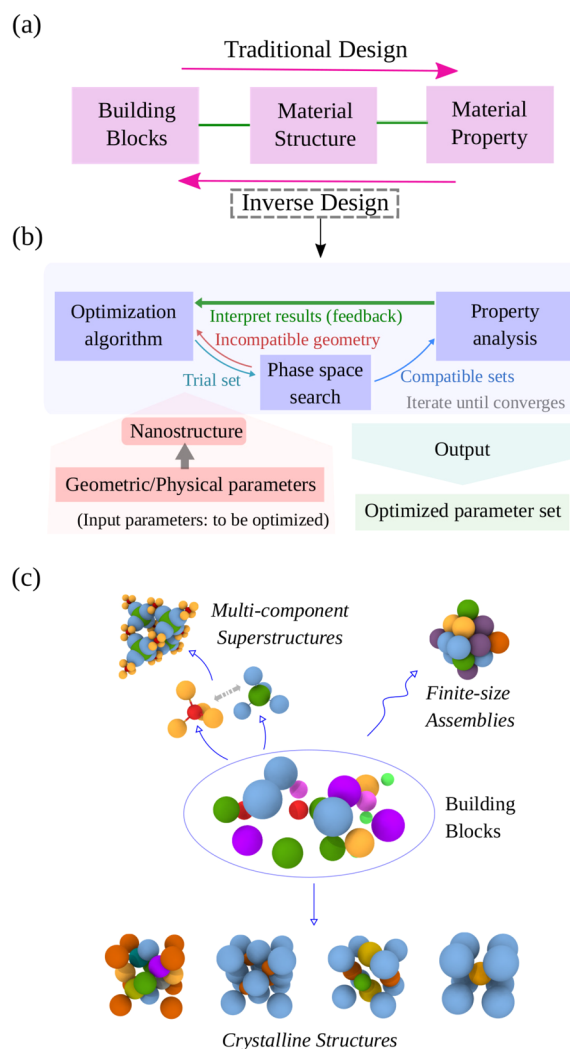


Figure 1. (a) Traditional vs inverse material design flowchart. (b) Schematic of GA-assisted inverse material design framework. (c) Example target structures for inverse material design framework originating from colloidal building blocks. Different colors refer to different types of particles with various sizes and properties.

which is not feasible with simple analytical methods and demands efficient computer algorithms.

Here we utilize the optimization framework shown in Figure 1b to find the set of geometric parameters and building block physical properties that will optimize target properties for different categories of colloidal structures. A wide range of these colloidal structures are considered excellent candidates as photonic metamaterials.^{47,62} Therefore, without loss of generality, we focus our GA-assisted inverse material design framework on the photonic properties of the colloidal structures. Under this paradigm, one starts with identifying the parameters that are relevant for reaching a desired property for a set of building blocks that form a specific structure. In the case of photonic property optimization, we consider the diameter (σ) and dielectric constant (ϵ) of each particle type. The first step toward finding an optimized set of parameters is to generate a trial set with entries from all parameters as input for the optimization algorithm. The next step in the optimization paradigm is to accept or reject the trial set based on its compatibility with the overall symmetry of target structure on the basis of its geometric properties. For an

accepted set, the structure is generated and evaluated for the target property. In this study, we demonstrate our GA-assisted scheme for two main categories of structures: (1) crystals of spherically symmetric colloidal particles and (2) multi-component superstructures of colloidal molecules where each building block is composed of a number of permanently bonded spherical particles. These classes of structures, in essence, provide samples of structures with simple as well as more complex building blocks to demonstrate the full scope of this inverse material design approach. We present this method in two steps: The first step involves the analysis of the geometric parameters to understand the geometric landscape and the geometric constraints that relate the overall structure to its building blocks. The second step is to investigate property–structure relations that guide the optimization of material properties within an inverse material design approach.

Geometric Phase Space. We begin by investigating the geometric landscape of various types of superstructures that can be formed from colloidal particles. A simple case involves spherically symmetric particles that can form binary crystalline structures. Before describing the geometric phase space for these systems, we note that the geometric solution space includes two degrees of freedom, with each particle type contributing to one degree of freedom: σ_i represents particle diameters where the subscript i refers to specific particle types (colors). The diameter of the particles must be selected in a way that when assembled, the target structure is achieved through establishing appropriate contacts between different particle types. This gives rise to the geometric phase diagram, which is calculated by considering the corresponding geometric constraints for each structure. For example, if a specific value for lattice parameter, a , is targeted for the CsCl structure shown in Figure 2a, the selection of particle diameters will be

functionalization, the particles may experience very short-range interactions, for example, for DNA-coated particles, or longer range interactions, for example, for particles coated by organic ligands.^{57,63,64}

The separation parameter $s = \frac{2l}{\sigma_1 + \sigma_2}$, defined based on the particle center-to-center distance l normalized by the average diameter of the particle pair $(\sigma_1 + \sigma_2)/2$, will thus be assumed to take a set of different values to reflect different possible interaction ranges. Figure 2a,b shows the results of geometric analysis for binary structures of spherical particles with cesium chloride (CsCl) and zincblende (ZnS) symmetries, for different values of s at 1.025 and 1.05. We assumed an example target lattice parameter of $a = 1000$ nm; however, the same approach can be used for systems with any other selection for the target lattice parameter. The two particle diameters for the x and y axis of the geometric phase space, σ_B and σ_Y , refer to the blue and yellow particles that need to establish proper contact for the formation of this structure. The blue and the red regions on the plots depict the acceptable domains for σ_B and σ_Y that satisfy the geometric constraints for the corresponding structures. We note that the blue domains are larger and cover the red domains, which implies that larger values for the separation parameter s , that is, longer effective interaction ranges, will result in a larger feasible domain in the geometric phase space. Although the results in Figure 2 apply to fairly simple structures, they provide a baseline for describing geometric phase space of more complex structures.

Next, we study colloidal constructs built from multi-component colloidal molecules. These structures involve more complex geometrical constraints than those made from simple spherical particles. The first system we study here is a superstructure grown via self-assembly of two types of clusters, cubic and octahedral,⁶⁵ where each cluster is formed from permanently bonded colloidal particles. A detailed picture of this construct is shown in Figure 3a. For this structure, the necessary geometric condition is achieved by establishing proper contact between the cubes and the octahedra for 4-fold blue–yellow directional interactions. Similar to the previous case, our algorithm navigates this 2-D phase space to find possible sets of (σ_B, σ_Y) that can deliver the desired superstructure shown in Figure 3a. The phase behavior is investigated for different values of separation parameter, s . We also introduce the maximum relative size ratio of the two particle types, r_{\max} , as another control parameter. Here, r_{\max} defines an upper threshold for the ratio of σ_B and σ_Y , while $1/r_{\max}$ sets the lower bound, thus providing the flexibility to limit the relative size of the two building block types within a desirable range. The sample phase diagram shown in Figure 3b evaluates the particle sizes within the range of 100–350 nm for different values of s and r_{\max} while assuming a lattice parameter of $a = 1000$ nm for the superstructure. The green, blue, and red regions show the feasible range of particle sizes for the formation of the superstructure. As expected, for larger values of separation parameter s , the feasible domain is larger. The black line corresponds to the idealized limit with $s = 1$, which relates to the case of an exact contact between two spheres without considering the soft interaction potential. In this case, the feasible region is reduced to a line and provides a purely geometric constraint that matches analytical geometric calculations. Figure 3c shows the variations of the feasible geometric domain with the lattice parameter of the superstructures. We observe that the general shape of the feasible

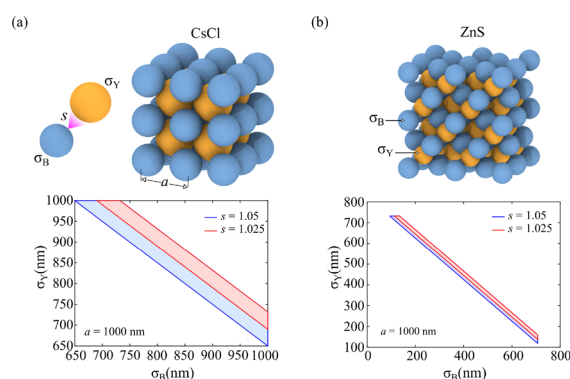


Figure 2. Geometric phase diagram for binary structures of spherical colloidal particles. σ_B and σ_Y refer to blue and yellow particle diameters; s specifies the distance between two particle surfaces corresponding to their equilibrium distance. The blue and red regions on the diagram show the feasible domain of σ_B and σ_Y for different values of s for (a) cesium chloride structure and (b) zincblende structure, both with a target lattice parameter of $a = 1000$ nm.

constrained by this lattice parameter and by the fact that a desired distance between the blue and yellow particles is needed for establishing proper contacts. This is essentially achieved when two particles are located within the equilibrium distance dictated by the interparticle interactions, i.e. the particle pairs are separated by a finite distance that is reflective of the effective interaction range when two particles are in equilibrium. Depending on the type of colloidal particle surface

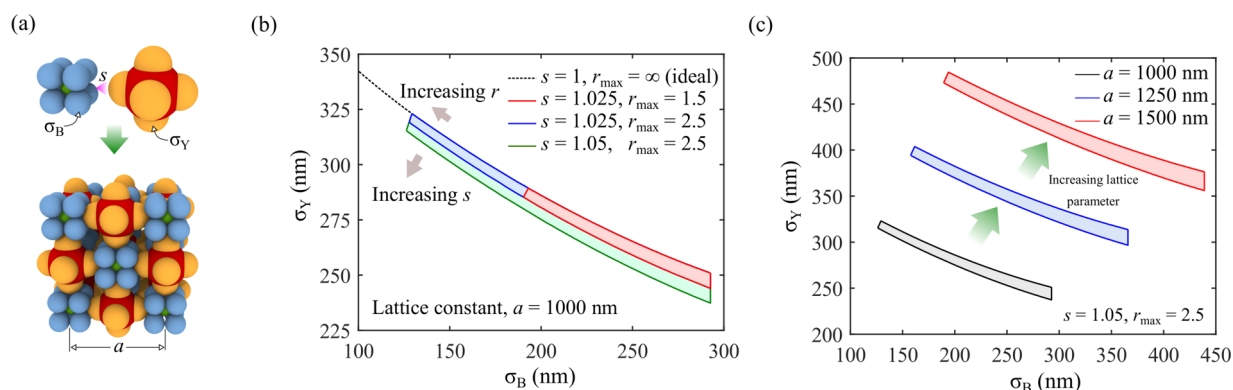


Figure 3. (a) Formation of cube-octahedron superstructure from self-assembly of two types of colloidal clusters. σ , s , and r_{\max} represents particle diameters, particle separation, and size ratio upper limit, respectively. (b) Geometric phase diagram of the superstructure for target lattice parameter of $a = 1000$ nm. (c) Variations of feasible region for different lattice parameters.

domain remains the same with changing target lattice parameter, which showcases the consistency of the geometric search algorithm used in this study.

We apply the same method to explore the geometric phase space of other types of superstructures. Figure 4 illustrates the resulting feasible domains for three other types of structures made through various combinations of tetrahedral building blocks. The first superstructure is a Laves phase, with MgSnCu_4 symmetry, formed by two types of spherical particles and one type of tetrahedral cluster.^{31,32} The second and third superstructures are diamond symmetries formed through assembly of tetrahedral and linear building blocks.⁶⁵ For the MgSnCu_4 structure, there are four relevant geometric parameters: the diameters of the three particle types, that is, σ_Y , σ_B , σ_R , and the sintering parameter, σ_{cc} , which defines possible overlap between (yellow) particles belonging to a tetrahedral unit. For the combinations of tetrahedral and linear units or the combination of two types of tetrahedra, three relevant geometric parameters, σ_Y , σ_B , and σ_R , are considered. Additionally, the geometry of individual tetrahedra imposes a condition on the relative size of yellow and red particles.⁶⁵ In essence, the structures are formed by carefully selecting the building blocks and the interactions among all possible particle pairs that are described by a set of inequalities during the analysis phase upon considering both the particle types and their relative positions. The resulting feasible geometric phase space for these structures reside in 3-D or 4-D (hyper) space and are shown as 2-D projections in Figure 4a–c for a few combinations of the corresponding parameters.

In order to provide a measure for the size of the feasible domain within geometric phase analysis, we introduce the Geometric Landscape Accessibility (GLA) parameter for a structure. GLA is defined as the ratio of the size of feasible domain to a reference domain such that the relative measurement can be compared across structures. In this regard, the base region formed by allowing each diameter to vary in the range $(0, a)$, that is, from zero to the value of lattice parameter, has been taken as the reference. For complex structures, this reference region would essentially be a hypercube of volume a^n where n is the number of relevant parameters. Figure 5 shows a summary of GLA values for superstructures introduced above, with the corresponding area or volume of the feasible domains approximated by a convex hull. We observe that the maximum GLA for the combination of cubic and octahedral structures is around 0.2%, while the

tetrahedral units show maximum geometric landscape accessibility of around 0.02%. This is consistent with the fact that for tetrahedral systems considered here, the size of the center red particles constitutes an additional geometric restriction that reduces the size of the feasibility domain. In general, for systems with higher numbers of geometric parameters or highly constrained geometry, we expect the GLA to be smaller. Furthermore, it is worth mentioning that with purely geometric constraints that disregard the interaction range, such as the case for the black line shown in Figure 3b, the feasible domains may be reduced to single lines or collections of lines, which reduces the GLA to zero. GLA can be interpreted as the relative difficulty in finding the geometrically feasible region inside the solution space. If the feasible region is unknown to the optimization algorithm, as is generally the case for complex structures, the algorithm starts searching from a random location, and for structures with lower GLA, it will spend considerable time outside the feasible domain during run-time. In reference to Figure 1b, many trial sets will be rejected by the geometric compatibility test, and only those consistent with geometric constraints will be evaluated for material properties.

Investigation of Structure–Property Relations. After exploring the geometric phase space and identifying feasible combinations of geometric parameters that guarantee the formation of the desired structures, we focus on target properties that derive from the inverse material design approach. Optimization algorithms used here adequately handle solution spaces that are presumably nondifferentiable and sparse in nature. As mentioned earlier, we explore photonic properties of the colloidal structures and specifically focus on finding structures that deliver target photonic band gap sizes. In reference to photonic properties, the solution space maps to photonic band gap sizes in a complex way dictated by the physical properties and the geometry of the building blocks. For a trial set of particle diameters generated by the algorithm mapped into the photonic band gap space, there are three possible scenarios that can happen. First, the target structure may not exist for the trial set due to geometric incompatibility, which produces an error in the compatibility test. In the second case, a structure may exist but that particular configuration may not have a band gap. Finally, the structure may have a band gap in which case it will be registered as a non-negative number. Metaheuristic methods

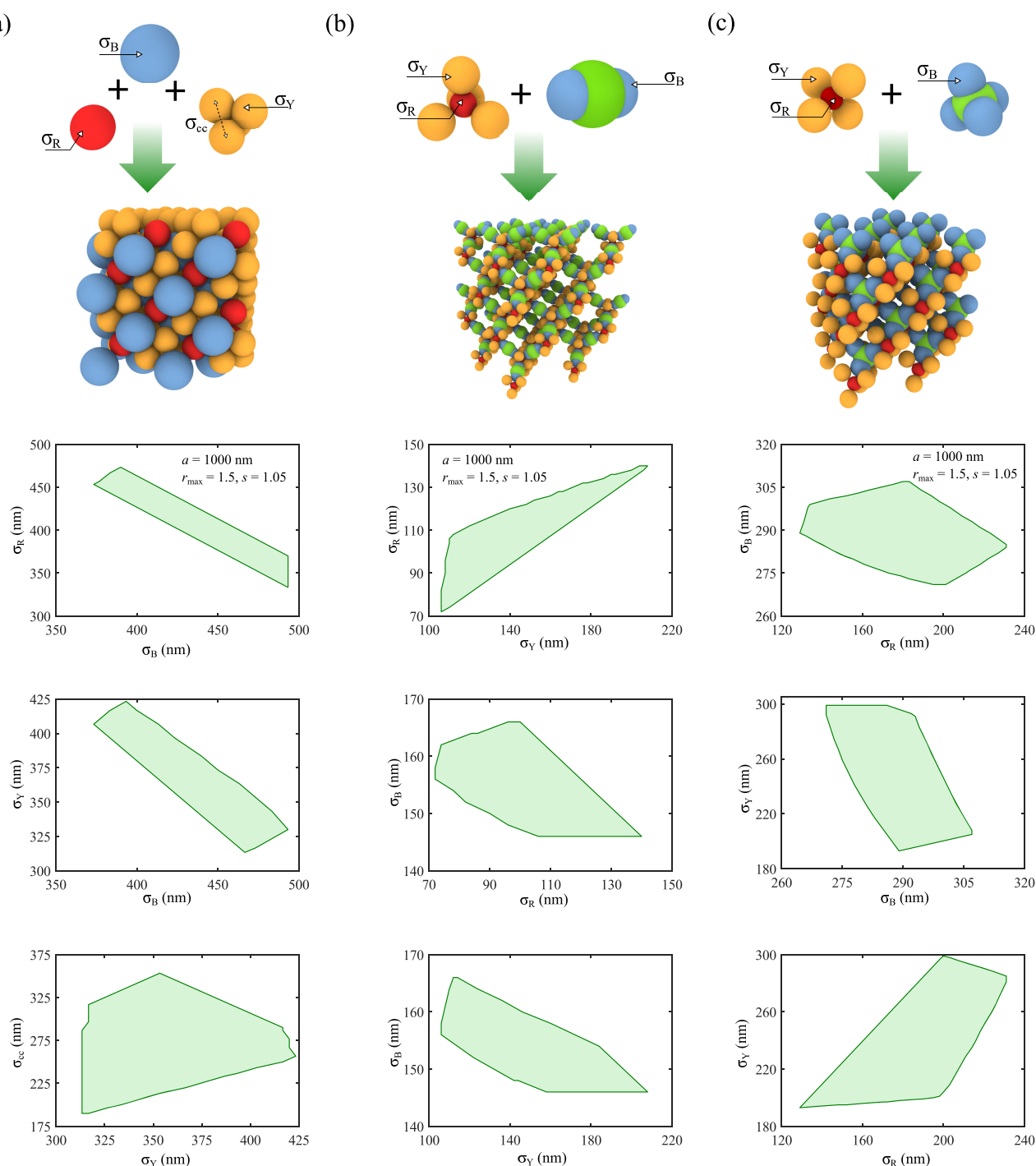


Figure 4. Geometric phase diagram for superstructures made with tetrahedral units, shown for particle separation $s = 1.05$ and size ratio upper limit $r_{\max} = 1.05$. σ_i refers to the particle diameter of color i . (a) MgSnCu_4 symmetry formed by two types of spherical particles and one type of tetrahedral cluster. (b) Superstructure formed by combination of tetrahedral and linear clusters. (c) Superstructure assembled from two types of tetrahedral clusters.

such as Genetic Algorithm (GA) are known to handle such spaces adequately well.

Each particle type within each structure introduces two degrees of freedom: σ_i representing particle size and ϵ_i representing the dielectric constant of the material for particle type i . Genetic Algorithm is used to explore various combinations of these parameters for each structure and detect the maximum photonic band gap size along with the corresponding σ and ϵ for each particle type. Particle size

combinations are constrained based on the geometry and interaction pattern, which are unique to the structure. For example, for the superstructures formed from two types of tetrahedral clusters, following the geometric phase space obtained in Figure 4c, the Genetic Algorithm generates a trial set with 4 values for particles diameters ($\sigma_R, \sigma_Y, \sigma_B, \sigma_G$) and 4 values for the material dielectric constants ($\epsilon_R, \epsilon_Y, \epsilon_B, \epsilon_G$), and subsequently calculates the photonic band gap corresponding to the overall superstructure with the selected

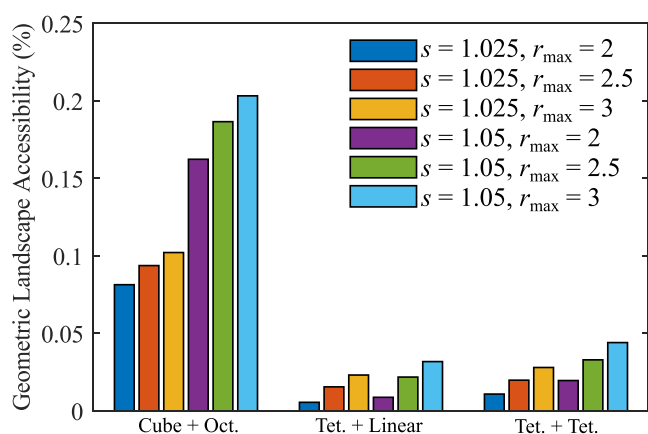


Figure 5. Geometric Landscape Accessibility (GLA) values calculated for different superstructures of colloidal clusters. “Tet.” and “Oct.” refer to tetrahedral and octahedral units, respectively, s refers to particle separation, and r_{\max} denotes maximum allowed particle size ratio.

parameters. The GA introduces the trial sets, called *generations*, in a batch to batch fashion and repeats this cycle until it finds the set of 8 parameters that optimize (maximize) the band gap size. Figure 6 demonstrates the outcome of GA-assisted optimization scheme for this superstructure. Employing the GA with an allowed diameter range of 100–400 nm at $a = 1000$ nm and dielectric constant values in the range of 2–18, we obtained the optimized parameter set shown in Figure 6a

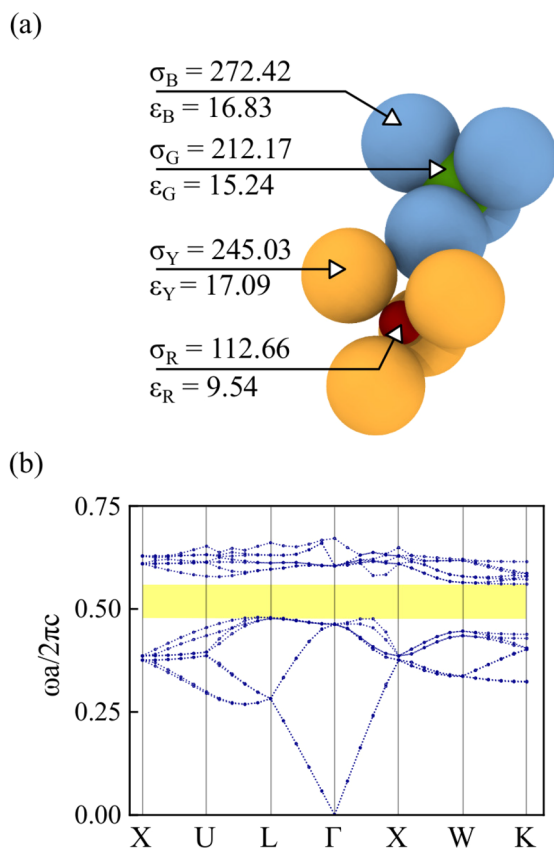


Figure 6. (a) Optimized parameters for Tet. + Tet. superstructure. (b) Corresponding band structure with maximized band gap size of 15.45%.

with maximum band gap size of 15.45% between the eighth and ninth bands within the photonic spectrum.

Considering other colloidal constructs discussed earlier, Figure 7 shows the optimization outcomes for different

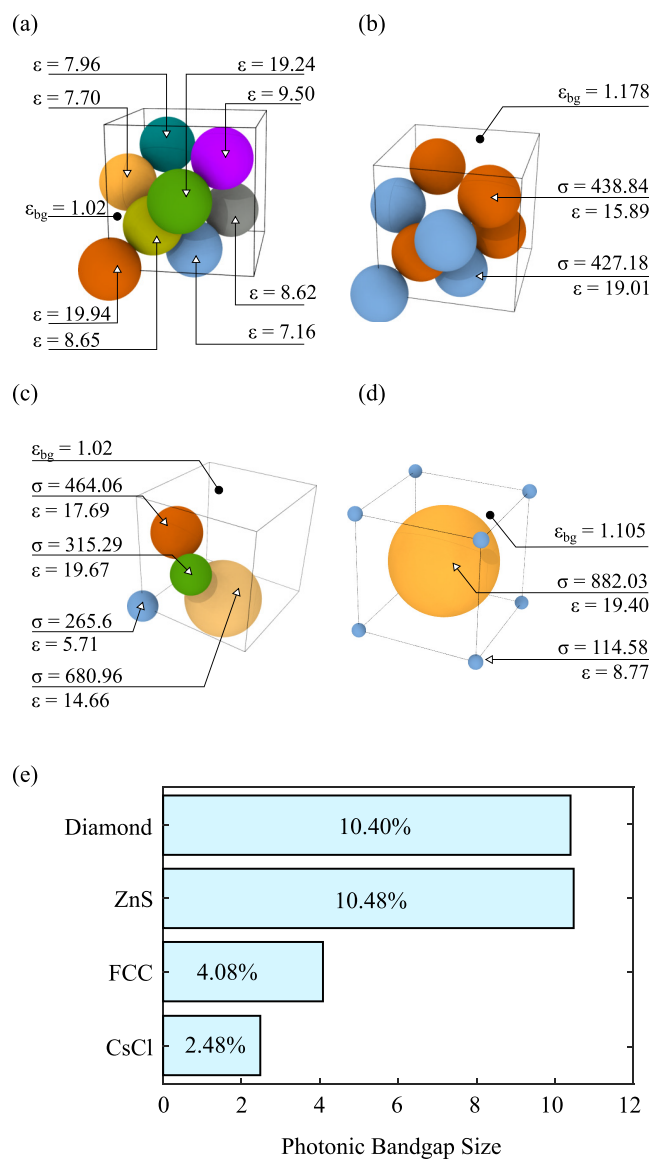


Figure 7. GA optimized structures of (a) diamond (packing factor 0.34), (b) ZnS (packing factor 0.34027), (c) FCC (packing factor 0.244), and (d) CsCl (packing factor 0.36) structures with the optimized value of the total band gap for the given configurations (e).

structures of simple spherical particles. For the diamond-like structures in Figure 7a, each particle has a diameter of $\sqrt{3}/4a$ allowing mutual contacts between the particles. The particles in the periodic unit cells are assumed to have dielectric constants different from the background material. In total, the search space has 9 independent dimensions. The GA analysis converges at a maximum band gap size of 10.40% for the parameter values shown in Figure 7a. This result shows that a significant departure from the native diamond structure is possible if various particle types exist within the unit cell that implement large variations in dielectric properties. In a similar manner, we consider the zincblende structure in a five dimensional optimization study. The parameter set includes

the dielectric constant of two types of particles as well as the background material and the diameters of blue and red particles. Confining the parameter search to the corresponding geometric phase space, we found a maximum band gap of 10.48% for the configuration in Figure 7b.

Next, to analyze a FCC-type structure, we allowed the genetic algorithm to modify both the diameters and dielectric properties of the particles, as well as the dielectric property of the background material, forming a 9 dimensional solution space for 4 particle types. As opposed to the other structures we discussed so far, here we eliminated the *close-packing* constraint to allow for more degrees of freedom, as non-close-packed assemblies of colloidal particles have been previously reported in a considerable number of studies in the literature. We explored particle diameters in the 50–1500 nm range and dielectric constants between 1 and 20. Contrary to the ideal FCC structure with one particle type that does not show any band gaps,⁶⁶ we found a band gap of 4.08% for the configuration shown in Figure 7c. Similarly, we analyzed the CsCl structure with BCC symmetry with five degrees of freedom. For this case shown in Figure 7d, the GA converged at a maximum band gap size of 2.48%.

Comparing the results obtained here for the TT structure to our previous study,⁶⁵ GA found a wider band gap for this structure at a dramatically reduced effort. In case of the diamond-like structures, the existence of a photonic band gap for this symmetry is well established.⁶⁷ In this study, however, we relaxed the constraints on the physical properties of the particles to explore other possibilities. The GA predicted diamond like configuration possesses a relative photonic band gap width of 9.54%, which puts this configuration at the upper limit of what has been obtained from “direct-diamond” structures made from colloids.⁶⁸ This flexibility is again realized for the case of FCC where the GA search reproduced the existence of complete photonic band gap for FCC at low filling fraction with no prior knowledge about the system.⁶⁹ Further advantage lies in the fact that a certain value of photonic band gap can be “targeted” to reverse engineer the refractive contrast requirements.

As mentioned previously, the Genetic Algorithm accesses the solution space in a sparse fashion. In Figure 8, the access pattern for diameter and dielectric property of blue particles from FCC structure and its background material is shown. The color bar shows when a set was picked by the GA and the height is a measurement of how often a certain value was selected. We observe that the GA accessed few values outside the allowed ranges. This is due to the statistical nature of trial set generation and was dealt with by assigning an error during compatibility test. It is also worth mentioning that GA rarely finds the true optimum solution and the definition of convergence is often a compromise between desired accuracy and computational effort. Additionally, similar to other optimization algorithms, the convergence rate can be slow or fast depending on the solution space, selection of GA related parameters, and starting point. For the structures considered in this study, the FCC case is, in fact, an example of slow convergence for the GA. The overall convergence occurred well after the 40th iteration, where convergence was declared once the population standard deviation of the target property values (fitness) became less than 0.5 for 5 successive generations. However, when focusing on the best candidate from each generation, the convergence pattern becomes clear within a few generations. The convergence pattern for a few of

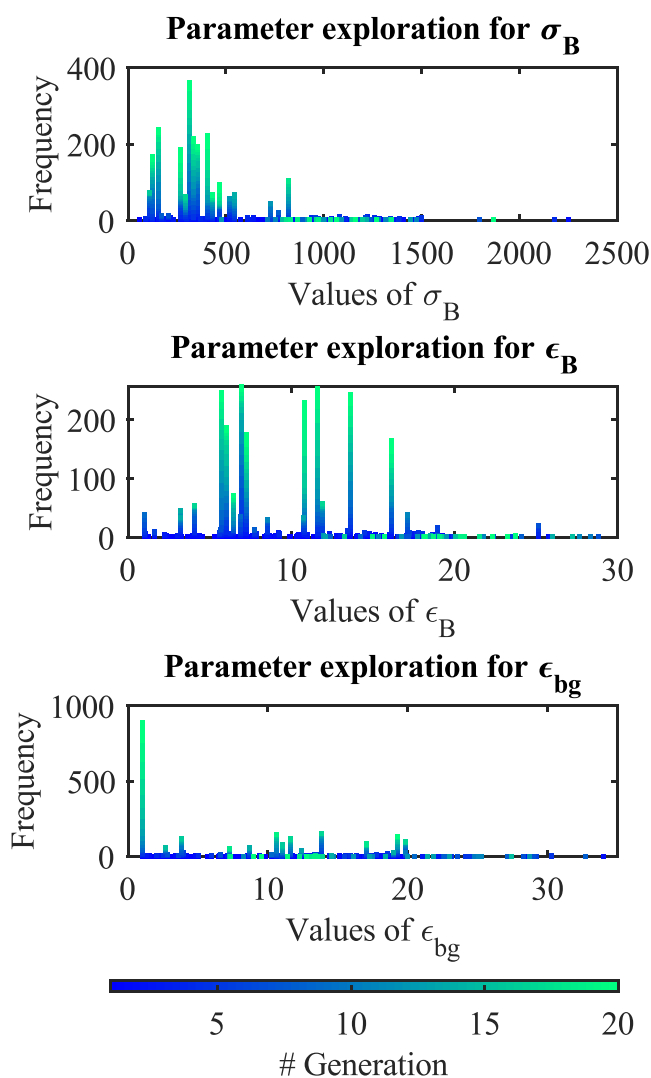


Figure 8. GA access pattern for the (a) diameter and (b) dielectric constant of the blue particles within the FCC structure and (c) the dielectric constant of the background material.

the structures in this study is provided in Figure 9. We note that the staircase-like shape of the fitness progression is a characteristic of the GA optimization scheme, and the rather unusual kinks in the plot for the cases of diamond and FCC structures is a result of allowing relatively larger population sizes and higher rates of mutation.

CONCLUSIONS

In summary, we established a GA-assisted framework to facilitate inverse material design with micro- and nanoscale colloidal building blocks. Target properties are the driving factor for this purpose, and the characteristics of the building blocks such as particle size and dielectric constant, are selected so that the overall structure exhibits the target property. We also demonstrated the accessible geometric phase space that limits the available choices for particle size and building block shape within the material design procedure, which is a direct result of the geometric constraints for different superstructures and symmetries. Based on the geometric constraints, we introduced Geometric Landscape Accessibility (GLA) as a measure of the size of the feasible domain within the geometric parameter space. We showed that for complex building blocks

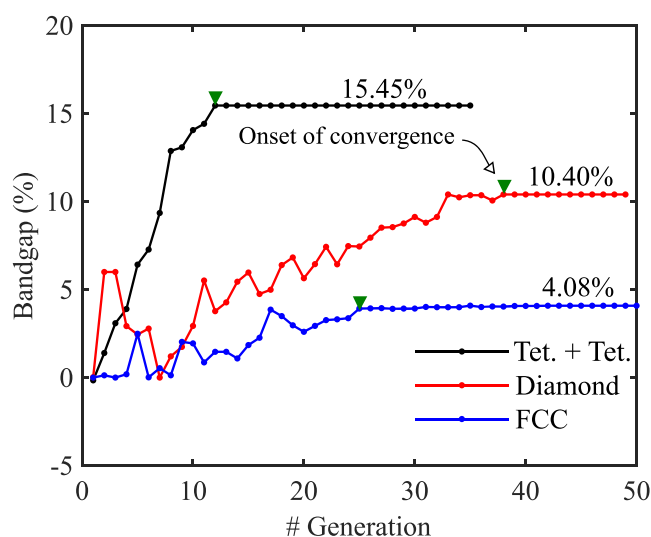


Figure 9. Fitness trend of best individual sets from each generation for three example structures. Green triangle shows the onset of convergence in the optimization process.

such as colloidal molecules, GLA turns out to be a typically small value below 1%. Furthermore, the geometric landscape often turns out to be quite complicated to be explored with analytical methods and thus needs to be investigated with efficient computer algorithms embedded within the GA-assisted material design framework. As demonstrated, the framework was utilized to optimize photonic band gap size of a variety of colloidal superstructures, constrained with the available values of geometric parameters dictated by the geometric phase space analysis. It is also worth mentioning that in this study only monodisperse crystalline phases have been considered. The presence of polydispersity can manifest itself in the form of structural defects or property variations across a single structure. Such effects may be accounted for by using stochastic methods embedded within the GA framework, which is beyond the scope of the tools used in this paper and needs to be investigated in detail in future studies. The strength of this approach lies in the fact that the same framework could be used to design structures with different types of target properties, including but not limited to materials with desired phononic, thermal, and mechanical characteristics. This work paves the way for future efforts to take advantage of Genetic Algorithm and machine-learning-based frameworks to streamline property-driven design of metamaterials with colloidal building blocks.

METHODS

For computing the geometrically feasible region, the geometric constraints are first expressed in terms of a set of inequalities by considering the diameter and coordinates of the associated particles at their desired locations. In the next step, we employ a brute force method to search the probable geometric region. A constraint that no particle in the structure can have a diameter larger than the lattice parameter is applied. Therefore, each diameter can assume a value between zero and the lattice parameter, a . Furthermore, the “area” or the “size” of the reference geometric region based on the maximum allowable limit for each diameter will be equal to a^n , where n represents the number of dimensions of the geometric space. Once the geometrically feasible regions are identified, we use convex hull

approximation to obtain the size of each region. The ratio of the size of the feasible region to the size of the reference region provides the GLA value. For example, in Figure 4 the GLA is calculated as the ratio of the area of the green region divided by 10^6 nm^2 for each case.

The GA-assisted material design framework was implemented in Python programming environment with Distributed Evolutionary Algorithms in Python (DEAP) package for Genetic Algorithm⁷⁰ implementation. During simulation, the population size was taken to be 32 for the Tet. + Tet. structure and 128 for all the other structures. Initial population was created using the built-in random number generator. Uniform crossover and Gaussian mutation with tournament selection (size = 2) were used throughout the test. Crossover and mutation rate for various structures varied between the values of 0.995, 0.005 and 0.95, 0.05. Photonic band structures were computed using MPB software package⁷¹ for the lowest 15 bands at $16 \times 16 \times 16$ grid with basis vectors along the Cartesian coordinates and along the critical points of the first Brillouin zone of the respective structures. Overall simulation time (based on convergence of best individual) ranged from about 6 CPU hours (Tet. + Tet. structure) to above 200 CPU hours (structures from Figure 7).

The major criterion that lead to acceptance or rejection of each trial set was its consistency with the geometric phase space of the desired structure and was closely linked to the existence and complexity of the geometric landscape test. For Tet. + Tet. structure, only 73% of the total sets were evaluated for property optimization due to geometric incompatibility of the rest of parameter sets. This percentage varies with generation and becomes almost 100% toward the end of the optimization steps. For diamond structure, this percentage was 100% throughout the whole run time (due to the absence of geometric compatibility test) except for rare cases of dielectric constant falling outside the allowed range. Overall, acceptance of a trial set within the GA cycle and the computational effort toward optimization is a function of solution space’s volume, dimension, and complexity, choice of GA parameters, definition of convergence, and desired accuracy and quality of the solution.

AUTHOR INFORMATION

Corresponding Author

*E-mail: zanjanm@miamioh.edu.

ORCID

Mehdi B. Zanjani: 0000-0003-3994-3420

Notes

The authors declare no competing financial interest.

ACKNOWLEDGMENTS

We acknowledge computational resources provided by the Ohio Supercomputer Center (Grant Number PMIU0139). We also acknowledge the support from Jens Mueller of the Research Computing group and the use of the Redhawk Cluster at Miami University.

REFERENCES

- (1) Rogers, W. B.; Shih, W. M.; Manoharan, V. N. Using DNA to Program the Self-Assembly of Colloidal Nanoparticles and Micro-particles. *Nat. Rev. Mater.* **2016**, *1*, 16008.

- (2) Damasceno, P. F.; Engel, M.; Glotzer, S. C. Predictive Self-Assembly of Polyhedra into Complex Structures. *Science (Washington, DC, U. S.)* **2012**, *337*, 453–457.
- (3) Travesset, A. Self-Assembly Enters the Design Era. *Science (Washington, DC, U. S.)* **2011**, *334*, 183–184.
- (4) Chen, Q.; Bae, S. C.; Granick, S. Directed Self-Assembly of a Colloidal Kagome Lattice. *Nature* **2011**, *469*, 381–385.
- (5) Casey, M. T.; Rogers, W. B.; Scarlett, R.; Jenkins, I.; Sinno, T.; Crocker, J. C. Driving Diffusionless Transformations in Colloidal Crystals using DNA Handshaking. *Nat. Commun.* **2012**, *3*, 1209.
- (6) Romano, F.; Sciortino, F. Patterning Symmetry in the Rational Design of Colloidal Crystals. *Nat. Commun.* **2012**, *3*, 1968.
- (7) Sztrum, C. G.; Hod, O.; Rabani, E. Self-Assembly of Nanoparticles in Three-Dimensions: Formation of Stalagmites. *J. Phys. Chem. B* **2005**, *109*, 6741–6747.
- (8) Edlund, E.; Lindgren, O.; Jacobi, M. N. Designing Isotropic Interactions for Self-Assembly of Complex Lattices. *Phys. Rev. Lett.* **2011**, *107*, 085503.
- (9) Srinivasan, B.; Vo, T.; Zhang, Y.; Gang, O.; Kumar, S.; Venkatasubramanian, V. Designing DNA-Grafted Particles that Self-Assemble into Desired Crystalline Structures using the Genetic Algorithm. *Proc. Natl. Acad. Sci. U. S. A.* **2013**, *110*, 18431–18435.
- (10) Jain, A.; Errington, J. R.; Truskett, T. M. Dimensionality and Design of Isotropic Interactions that Stabilize Honeycomb, Square, Simple Cubic, and Diamond Lattices. *Phys. Rev. X* **2014**, *4*, 031049.
- (11) Vo, T.; Venkatasubramanian, V.; Kumar, S.; Srinivasan, B.; Pal, S.; Zhang, Y.; Gang, O. Stoichiometric Control of DNA-Grafted Colloid Self-Assembly. *Proc. Natl. Acad. Sci. U. S. A.* **2015**, *112*, 4982–4987.
- (12) Luo, B.; Kim, A.; Smith, J. W.; Ou, Z.; Wu, Z.; Kim, J.; Chen, Q. Hierarchical Self-Assembly of 3D Lattices from Polydisperse Anisotropic Colloids. *Nat. Commun.* **2019**, *10*, 1815.
- (13) Ou, Z.; Luo, B.; Neophytou, A.; Chakrabarti, D.; Chen, Q. Synthesis and Self-Assembly of Janus and Triblock Patchy Particles. *Front. Nanosci.* **2019**, *13*, 61–85.
- (14) Luo, B.; Smith, J. W.; Wu, Z.; Kim, J.; Ou, Z.; Chen, Q. Polymerization-Like Co-Assembly of Silver Nanoplates and Patchy Spheres. *ACS Nano* **2017**, *11*, 7626–7633.
- (15) Chen, Q.; Yan, J.; Zhang, J.; Bae, S. C.; Granick, S. Janus and Multiblock Colloidal Particles. *Langmuir* **2012**, *28*, 13555–13561.
- (16) Moaseri, E.; Bollinger, J. A.; Changalvaie, B.; Johnson, L.; Schroer, J.; Johnston, K. P.; Truskett, T. M. Reversible Self-Assembly of Glutathione-Coated Gold Nanoparticle Clusters via pH-Tunable Interactions. *Langmuir* **2017**, *33*, 12244–12253.
- (17) Bachhar, N.; Jiao, Y.; Asai, M.; Akcora, P.; Bandyopadhyaya, R.; Kumar, S. K. Impact of the Distributions of Core Size and Grafting Density on the Self-Assembly of Polymer Grafted Nanoparticles. *Macromolecules* **2017**, *50*, 7730–7738.
- (18) Zhang, Z.; Keys, A. S.; Chen, T.; Glotzer, S. C. Self-Assembly of Patchy Particles into Diamond Structures through Molecular Mimicry. *Langmuir* **2005**, *21*, 11547–11551.
- (19) Sztrum-Vartash, C. G.; Rabani, E. Lattice Gas Model for the Drying-Mediated Self-Assembly of Nanorods. *J. Phys. Chem. C* **2010**, *114*, 11040–11049.
- (20) Kraft, D. J.; Ni, R.; Smallenburg, F.; Hermes, M.; Yoon, K.; Weitz, D. A.; van Blaaderen, A.; Groenewold, J.; Dijkstra, M.; Kegel, W. K. Surface Roughness Directed Self-Assembly of Patchy Particles into Colloidal Micelles. *Proc. Natl. Acad. Sci. U. S. A.* **2012**, *109*, 10787–10792.
- (21) Bianchi, E.; Blaak, R.; Likos, C. N. Patchy Colloids: State of the Art and Perspectives. *Phys. Chem. Chem. Phys.* **2011**, *13*, 6397–6410.
- (22) Sacanna, S.; Korpics, M.; Rodriguez, K.; Colón-Meléndez, L.; Kim, S.-H.; Pine, D. J.; Yi, G.-R. Shaping Colloids for Self-Assembly. *Nat. Commun.* **2013**, *4*, 1688.
- (23) Wang, Y.; Hollingsworth, A. D.; Yang, S. K.; Patel, S.; Pine, D. J.; Weck, M. Patchy Particle Self-Assembly via Metal Coordination. *J. Am. Chem. Soc.* **2013**, *135*, 14064–14067.
- (24) Grunwald, M.; Geissler, P. L. Patterns without Patches: Hierarchical Self-Assembly of Complex Structures from Simple Building Blocks. *ACS Nano* **2014**, *8*, 5891–5897.
- (25) McGinley, J. T.; Jenkins, I.; Sinno, T.; Crocker, J. C. Assembling Colloidal Clusters using Crystalline Templates and Reprogrammable DNA Interactions. *Soft Matter* **2013**, *9*, 9119–9128.
- (26) van Anders, G.; Ahmed, N. K.; Smith, R.; Engel, M.; Glotzer, S. C. Entropically Patchy Particles: Engineering Valence through Shape Entropy. *ACS Nano* **2014**, *8*, 931–940.
- (27) McGinley, J. T.; Wang, Y.; Jenkins, I. C.; Sinno, T.; Crocker, J. C. Crystal-Templated Colloidal Clusters Exhibit Directional DNA Interactions. *ACS Nano* **2015**, *9*, 10817–10825.
- (28) Pattabhiraman, H.; Avvisati, G.; Dijkstra, M. Novel Pyrochlore-like Crystal with a Photonic Band Gap Self-Assembled Using Colloids with a Simple Interaction Potential. *Phys. Rev. Lett.* **2017**, *119*, 157401.
- (29) Avvisati, G.; Dasgupta, T.; Dijkstra, M. Fabrication of Colloidal Laves Phases via Hard Tetramers and Hard Spheres: Bulk Phase Diagram and Sedimentation Behavior. *ACS Nano* **2017**, *11*, 7702–7709.
- (30) Zanjani, M. B.; Jenkins, I. C.; Crocker, J. C.; Sinno, T. Colloidal Cluster Assembly into Ordered Superstructures via Engineered Directional Binding. *ACS Nano* **2016**, *10*, 11280–11289.
- (31) Zanjani, M. B.; Crocker, J. C.; Sinno, T. Self-Assembly with Colloidal Clusters: Facile Crystal Design using Connectivity Landscape Analysis. *Soft Matter* **2017**, *13*, 7098–7105.
- (32) Ducrot, É.; He, M.; Yi, G.-R.; Pine, D. J. Colloidal Alloys with Preassembled Clusters and Spheres. *Nat. Mater.* **2017**, *16*, 652–657.
- (33) Wang, D.; Hermes, M.; Kotni, R.; Wu, Y.; Tasios, N.; Liu, Y.; de Nijs, B.; van der Wee, E. B.; Murray, C. B.; Dijkstra, M.; van Blaaderen, A. Interplay Between Spherical Confinement and Particle Shape on the Self-Assembly of Rounded Cubes. *Nat. Commun.* **2018**, *9*, 2228.
- (34) Dasgupta, T.; Dijkstra, M. Towards the Colloidal Laves Phase from Binary Hard-Sphere Mixtures via Sedimentation. *Soft Matter* **2018**, *14*, 2465–2475.
- (35) Haji-Akbari, A.; Engel, M.; Keys, A. S.; Zheng, X.; Petschek, R. G.; Palfy-Muhoray, P.; Glotzer, S. C. Disordered, Quasicrystalline and Crystalline Phases of Densely Packed Tetrahedra. *Nature* **2009**, *462*, 773.
- (36) Haji-Akbari, A.; Engel, M.; Glotzer, S. C. Phase Diagram of Hard Tetrahedra. *J. Chem. Phys.* **2011**, *135*, 194101.
- (37) Haji-Akbari, A.; Chen, E. R.; Engel, M.; Glotzer, S. C. Packing and Self-Assembly of Truncated Triangular Bipyramids. *Phys. Rev. E* **2013**, *88*, 012127.
- (38) Asher, S. A.; Holtz, J.; Liu, L.; Wu, Z. Self-Assembly Motif for Creating Submicron Periodic Materials. Polymerized Crystalline Colloidal Arrays. *J. Am. Chem. Soc.* **1994**, *116*, 4997–4998.
- (39) Ye, Y. H.; LeBlanc, F.; Haché, A.; Truong, V. V. Self-Assembling Three-Dimensional Colloidal Photonic Crystal Structure with High Crystalline Quality. *Appl. Phys. Lett.* **2001**, *78*, 52–54.
- (40) Kitaev, V.; Ozin, G. A. Self-Assembled Surface Patterns of Binary Colloidal Crystals. *Adv. Mater.* **2003**, *15*, 75–78.
- (41) Wang, Y.; Wang, Y.; Zheng, X.; Ducrot, É.; Yodh, J. S.; Weck, M.; Pine, D. J. Crystallization of DNA-Coated Colloids. *Nat. Commun.* **2015**, *6*, 7253.
- (42) Geng, Y.; van Anders, G.; Glotzer, S. C. Predicting Colloidal Crystals from Shapes via Inverse Design and Machine Learning. arXiv Preprint arXiv:1801.06219 2018, <https://arxiv.org/abs/1801.06219>.
- (43) van Anders, G.; Ahmed, N. K.; Smith, R.; Engel, M.; Glotzer, S. C. Entropically Patchy Particles: Engineering Valence through Shape Entropy. *ACS Nano* **2014**, *8*, 931–940.
- (44) Haji-Akbari, A.; Glotzer, S. C. Strong Orientational Coordinates and Orientational Order Parameters for Symmetric Objects. *J. Phys. A: Math. Theor.* **2015**, *48*, 485201.
- (45) Subramanian, G.; Manoharan, V. N.; Thorne, J. D.; Pine, D. J. Ordered Macroporous Materials by Colloidal Assembly: A Possible Route to Photonic Bandgap Materials. *Adv. Mater.* **1999**, *11*, 1261–1265.

- (46) Manoharan, V. N.; Imhof, A.; Thorne, J. D.; Pine, D. J. Photonic Crystals from Emulsion Templates. *Adv. Mater.* **2001**, *13*, 447–450.
- (47) Joannopoulos, J. D.; Johnson, S. G.; Winn, J. N.; Meade, R. D. *Photonic Crystals: Molding the Flow of Light*; Princeton University Press, 2011.
- (48) Froufe-Pérez, L. S.; Engel, M.; Damasceno, P. F.; Muller, N.; Haberko, J.; Glotzer, S. C.; Scheffold, F. Role of Short-Range Order and Hyperuniformity in the Formation of Band Gaps in Disordered Photonic Materials. *Phys. Rev. Lett.* **2016**, *117*, 053902.
- (49) Davis, B. L.; Hussein, M. I. Nanophononic Metamaterial: Thermal Conductivity Reduction by Local Resonance. *Phys. Rev. Lett.* **2014**, *112*, 055505.
- (50) Hussein, M. I.; Leamy, M. J.; Ruzzene, M. Dynamics of Phononic Materials and Structures: Historical Origins, Recent Progress and Future Outlook. *Appl. Mech. Rev.* **2014**, *66*, 040802.
- (51) Han, T.; Bai, X.; Thong, J. T. L.; Li, B.; Qiu, C.-W. Full Control and Manipulation of Heat Signatures: Cloaking, Camouflage and Thermal Metamaterials. *Adv. Mater.* **2014**, *26*, 1731–1734.
- (52) Shipway, A. N.; Katz, E.; Willner, I. Nanoparticle Arrays on Surfaces for Electronic, Optical, and Sensor Applications. *ChemPhysChem* **2000**, *1*, 18–52.
- (53) McConnell, W. P.; Novak, J. P.; Brousseau, L. C.; Fuierer, R. R.; Tenent, R. C.; Feldheim, D. L. Electronic and Optical Properties of Chemically Modified Metal Nanoparticles and Molecularly Bridged Nanoparticle Arrays. *J. Phys. Chem. B* **2000**, *104*, 8925–8930.
- (54) Riniker, S. Molecular Dynamics Fingerprints (MDFP): Machine Learning from MD Data To Predict Free-Energy Differences. *J. Chem. Inf. Model.* **2017**, *57*, 726–741.
- (55) Sharpe, C.; Seepersad, C. C.; Watts, S.; Tortorelli, D. Design of Mechanical Metamaterials via Constrained Bayesian Optimization. *ASME 2018 Int. Des. Eng. Technol. Conf. Comput. Inf. Eng. Conf.* **2018**, V02AT03A029–V02AT03A029.
- (56) Spellings, M.; Glotzer, S. C. Machine Learning for Crystal Identification and Discovery. *AIChE J.* **2018**, *64*, 2198–2206.
- (57) Ducrot, E.; Gales, J.; Yi, G.-R.; Pine, D. Pyrochlore lattice, self-assembly and photonic band gap optimizations. *Opt. Express* **2018**, *26*, 30052–30060.
- (58) Courtney, T. H. Fundamental Structure-Property Relationships in Engineering Materials. *Mater. Sel. Des.* **1997**, *20*, 336.
- (59) Rogers, D.; Hopfinger, A. J. Application of Genetic Function Approximation to Quantitative Structure-Activity Relationships and Quantitative Structure-Property Relationships. *J. Chem. Inf. Model.* **1994**, *34*, 854–866.
- (60) Paik, T.; Murray, C. B. Shape-Directed Binary Assembly of Anisotropic Nanoplates: A Nanocrystal Puzzle with Shape-Complementary Building Blocks. *Nano Lett.* **2013**, *13*, 2952.
- (61) Rossi, L.; Sacanna, S.; Irvine, W. T. M.; Chaikin, P. M.; Pine, D. J.; Philipse, A. P. Cubic Crystals from Cubic Colloids. *Soft Matter* **2011**, *7*, 4139–4142.
- (62) Stimulak, M.; Ravník, M. Tunable Photonic Crystals with Partial Bandgaps from Blue Phase Colloidal Crystals and Dielectric-Doped Blue Phases. *Soft Matter* **2014**, *10*, 6339–6346.
- (63) Rogers, W. B.; Crocker, J. C. Direct Measurements of DNA-Mediated Colloidal Interactions and their Quantitative Modeling. *Proc. Natl. Acad. Sci. U. S. A.* **2011**, *108*, 15687–15692.
- (64) Dong, A.; Ye, X.; Chen, J.; Murray, C. B. Two-Dimensional Binary and Ternary Nanocrystal Superlattices: The Case of Monolayers and Bilayers. *Nano Lett.* **2011**, *11*, 1804–1809.
- (65) Aryana, K.; Stahley, J. B.; Parvez, N.; Kim, K.; Zanjani, M. B. Superstructures of Multielement Colloidal Molecules: Efficient Pathways to Construct Reconfigurable Photonic and Phononic Crystals. *Adv. Theory Simulations* **2019**, *2*, 1800198.
- (66) Ho, K. M.; Chan, C. T.; Soukoulis, C. M. Existence of a Photonic Gap in Periodic Dielectric Structures. *Phys. Rev. Lett.* **1990**, *65*, 3152–3155.
- (67) Maldovan, M.; Thomas, E. L. Diamond-Structured Photonic Crystals. *Nat. Mater.* **2004**, *3*, 593–600.
- (68) Hynninen, A. P.; Thijssen, J. H. J.; Vermolen, E. C. M.; Dijkstra, M.; Van Blaaderen, A. Self-assembly Route for Photonic Crystals with a Bandgap in the Visible Region. *Nat. Mater.* **2007**, *6*, 202–205.
- (69) Biswas, R.; Sigalas, M.; Subramania, G.; Ho, K. Photonic Band Gaps in Colloidal Systems. *Phys. Rev. B: Condens. Matter Mater. Phys.* **1998**, *57*, 3701–3705.
- (70) Fortin, F.-A.; De Rainville, F.-M.; Gardner, M.-A.; Parizeau, M.; Gagné, C. DEAP: Evolutionary Algorithms Made Easy. *J. Mach. Learn. Res.* **2012**, *13*, 2171–2175.
- (71) Johnson, S. G.; Joannopoulos, J. D. Block-Iterative Frequency-Domain Methods for Maxwell's Equations in a Planewave Basis. *Opt. Express* **2001**, *8*, 173–190.